Structural basis and functional roles for Toll-like receptor binding to Latrophilin adhesion-GPCR in embryo development

Gabriel Carmona Rosas[1,2,3,+], Jingxian Li[1,2,3,+], Jayson J. Smith[2,4,+], Shouqiang Cheng[1,2,3], Elana Baltrusaitis[1,2,3], Wioletta I. Nawrocka[1,2,3], Minglei Zhao[1], Paschalis Kratsios[2,4], Demet Araç[1,2,3,], and Engin Özkan[1,2,3,*]

1 Department of Biochemistry and Molecular Biology, The University of Chicago, Chicago, IL 60637 USA

2 Neuroscience Institute, The University of Chicago, Chicago, IL, 60637 USA

3 Institute for Biophysical Dynamics, The University of Chicago, Chicago, IL, 60637 USA

4 Department of Neurobiology, The University of Chicago, Chicago, IL 60637 USA

+ Co-first authors

* Correspondence: eozkan@uchicago.edu

Keywords:

Abstract

Latrophilins/ADGRLs are conserved adhesion-type G protein-coupled receptors associated with early embryonic morphogenesis defects, embryonic lethality, and sterility across multiple model organisms. However, their mechanistic roles in embryogenesis and the identity of their binding ligands remain unknown. Here, we show that *C. elegans* Latrophilin, LAT-1, directly interacts with the *C. elegans* Tol-like receptor, TOL-1. The N-terminal lectin domain of LAT-1 binds to the second leucine-rich repeat domain of TOL-1 with high affinity. The cryo-EM density map and the higher-resolution crystal structure of a 1:1 LAT-1–TOL-1 ectodomain complex reveal an unusual mode of interaction, the mutagenesis of which abolished binding *in vitro*. CRISPR/Cas9-mediated mutation of key residues selectively disrupted the endogenous LAT-1–TOL-1 interaction in *C. elegans,* leading to partial sterility, lethality, and malformed embryos. Thus, TOL-1 binding to LAT-1 represents a receptor-ligand axis essential for animal morphogenesis.

INTRODUCTION

During animal development, cells communicate with each other to follow a sequence of precisely controlled cell division events and to spatially arrange in a coordinated manner forming the embryo. Cellular communication during this process is mediated by cell-surface receptors that are believed to be conserved across animals. Several key cell-surface receptors mediate extracellular protein-protein interactions to induce signaling pathways acting at different times and in different regions of the embryo.[1] However, the molecular mechanisms of cellular communication that govern early embryogenesis are incompletely understood.

Latrophilins (LPHNs/ADGRLs) are cell-surface receptors with essential functions in animal development, especially in early embryogenesis, in both vertebrates and invertebrates.[2,3] They are signaling receptors of the adhesion G-protein-coupled receptor (aGPCR) family, found in all multicellular animals.[4–7] Among the 33 aGPCRs in humans, LPHNs (LPHN1-3) are the only aGPCRs, besides flamingo-like Cadherin EGF LAG seven-pass G-type receptors (CELSRs), that are conserved between vertebrates and invertebrates.[8] LPHNs have large extracellular domains (ECDs) comprised of a Lectin, an Olfactomedin (absent in *C. elegans* homolog LAT-1), a Hormone-Binding and a GAIN domain, which precedes the transmembrane (7TM) region **(Fig. 1A)**.[9–11]

The roles of LPHNs in embryonic development have been mostly studied in *C. elegans*, whose genome contains two LPHN orthologs, *lat-1* and lat-2. Although the function of lat-2 remains unknown, lat-1 is essential for early development; it is required for the alignment of cell division planes along the anterior-posterior axis.[12] *lat-1* is expressed in early blastomeres, developing embryonic epithelia, specifically in left epidermoblasts during dorsal intercalation, in pharyngeal muscles and neurons, and in the nerve ring.[12,13] Its expression is needed for embryo elongation, pharyngeal development, and sperm development and/or function. *lat-1* null mutant

worms display embryonic and larval lethality phenotypes (17% and 56%). Mice carrying homozygous null *Lphn1*[14,15] or *Lphn2*[16] alleles also show embryonic lethality, indicating that LPHN function in embryogenesis is conserved between invertebrates and vertebrates. Finally, numerous recent studies suggest roles for LPHNs in tissue physiology, such as heart development,[17] insulin secretion,[18] multidrug resistance in acute myeloid leukemia,[19] endothelial cell adhesion,[20] cardiac lineage commitment[21] and epithelial proliferation.[22] LPHNs are associated with developmental and neurobiological defects,[15] attention deficit hyperactivity disorder (ADHD)[23] and cancers.[23–26] However, the molecular mechanisms underlying LPHN function in development remain unknown.

Latrophilins have several known ligands. In vertebrate neurons, the extracellular domains of LPHNs interact with Teneurins (TENs) in a trans-synaptic manner and regulate excitatory synapse formation and organization.[6,16,27–36] TENs are large cell-surface proteins essential for gastrulation and epithelial to mesenchymal transition (in mice), heart and brain development (in flies), and the correct formation of basement membranes (in worms). Although, LPHNs and TENs are both key molecules for embryonic development, genetic interaction data for *lat-1* and *ten-1* mutant animals suggested that they act in parallel pathways during embryonic development.[13] LAT-1 and TEN-1 also appear to be expressed in the same cells, conflicting with a model where interactions between neighboring cells dictate tissue polarity and cell migrations in development. These results altogether implied that LPHNs and TENs may act in parallel on the same cell (*cis*), rather than on neighboring cells (*trans*) and suggested that other yet-to-be-described ligands of LPHNs mediate intercellular interactions for their functions in development.[2] Vertebrate LPHNs also interact with Fibronectin Leucine Rich Repeat Transmembrane Proteins (FLRTs) to mediate neuronal functions,[37,38] but FLRTs do not exist in invertebrates, and thus are likely not involved in the fundamental developmental roles of LPHNs. A recent work reported that *Drosophila* LPHN (Cirl) cooperates with Toll-8 to control

planar polarity in embryos.[39] The various roles of LPHNs in development and the numerous adhesion domains in their extracellular regions further suggest interaction with other ligands.

Here, we aimed to understand the mechanisms of action for LPHNs in their essential but relatively unstudied roles, especially in embryogenesis. To identify proteins that interact with LPHNs, we turned to *C. elegans*, which provides a powerful genetic model to study early development. Importantly, C. elegans animals lacking lat-1 (LPHN) display strong developmental phenotypes. Using our extracellular protein interaction discovery platform in *C. elegans*, we identified a cell-surface receptor, TOL-1 (Toll-like receptor/TLR), the sole Toll-like receptor in *C. elegans*, as a novel binding partner for LAT-1. *tol-1* has similar embryonic phenotypes as *lat-1*. To test whether Toll-like receptors mediate LPHN functions such as embryogenesis, in animals, we employed a multidisciplinary approach to study the function of this interaction: We determined the high-resolution crystal structure of the LAT-1–TOL-1 complex that is consistent with the cryo-EM density map of the full-length complex, and engineered point mutants at the binding interface to break the complex *in vitro*. We then used CRISPR/Cas9 and generated worms that carry homozygous alleles of *tol-1* or *lat-1* with point mutations that specifically disrupt the LAT-1–TOL-1 interaction. These genetic manipulations in C. elegans resulted in developmental defects similar to the ones observed in *tol-1* and *lat-1* null mutant animals. Our study suggests that the TOL-1–LAT-1 interaction is critical for early development in *C. elegans,* and likely in all animals.

RESULTS

LAT-1 interacts with the Toll-like receptor in *C. elegans*

To reveal novel interactors for LPHNs and study them in a well-established genetic model system, we chose to work with the nematode *C. elegans*, which provides several advantages: (1) Most conserved cell surface receptor families have fewer members in nematodes, allowing for less extensive screens to cover the putative interaction space. (2) There are only two *C. elegans* LPHN genes, *lat-1* and *lat-2*, but only *lat-1* mutants show major developmental phenotypes, circumventing potential redundancy issues as lat-2 appears unable to compensate for genetic loss of lat-1. (3) There is strong functional conservation to vertebrate LPHNs, where known phenotypes in nematodes match those in mice, including embryonic lethality. (4) Finally, embryonic development is easily tractable in C. elegans, compared to mammals.

We included the LAT-1 ectodomain in a protein interaction screen designed to discover extracellular interactions. The high-throughput assay, the Extracellular Interactome Assay (ECIA), uses an ELISA-like setup, where Fc-tagged bait are captured on solid support, and Alkaline phosphatase (AP)-tagged prey report on binding to the bait using chromogenic AP substrates **(Supplementary Fig. 1A)**.[40–42] Crucial to the sensitivity of the assay are high-density display of the bait on plastic support, matched by the oligomerization of the prey using a pentameric coiled coil, resulting in avidity and a large increase in sensitivity of the assay.[41,43] We tested LAT-1 against a library of 379 *C. elegans* ectodomains, chosen on the basis of domain content known to be conserved and important in developmental functions across bilaterians. The LAT-1-Fc bait captured TOL-1-AP prey with the highest significance across the entire library (**Fig. 1B**). Similarly, when TOL-1-Fc was used as bait, LAT-1-AP gave the strongest binding signal (**Fig. 1C**). TOL-1 is a cell surface receptor with two extracellular Leucine-Rich

Repeat (LRR) domains, one TM helix and a cytoplasmic Toll-Interleukin receptor-1 receptor (TIR) domain **(Fig. 1D)**.[44] Overall, these results identified the Toll-like receptor TOL-1 ECD as a binding partner for LAT-1 ECD.

Existing literature on nematode *lat-1* and *tol-1* demonstrate that these two genes may have roles in closely related developmental functions. In *C. elegans*, *tol-1* mutants show phenotypes in early development similar to those of *lat-1* animals.[45] Null *tol-1(nr2013)* mutant animals have high rates of arrest during embryonic development, high (larval?) mortality, and infertility. Expression patterns of *tol-1* in embryo suggest early roles in morphogenesis, while expression in adults is mostly neuronal,[45] similar to *lat-1* in adults.[12]

The LAT-1–TOL-1 interaction is direct and stoichiometric

To validate the direct interaction between LAT-1 and TOL-1 with orthogonal protein binding experiments, we created baculoviruses that express constructs covering LAT-1 and TOL-1 ECDs and purified these proteins. The full-length ECD of LAT-1, including the Lectin, HormR and GAIN domains, formed a highly stable complex with the full-length ECD of TOL-1 including the first and second LRR domains, as we observed a shift to the left in the elution volume of a mixed TOL-1–LAT-1 sample compared to the purified TOL-1 ectodomain and the LAT-1 ectodomain individually as analyzed by size-exclusion chromatography (SEC) **(Fig. 1E)**. The co-elution of both proteins was confirmed by SDS PAGE analysis **(Fig. 1E)**. These results confirmed the high-affinity interaction of LAT-1 with TOL-1.

To determine the exact molecular weight of the complex species that is observed on the size exclusion chromatogram, we used multi-angle light scattering (MALS) and calculated the observed molecular weight as 172 kDa (expected 171.1 kDa) corresponding to a 1:1 stoichiometry **(Fig. 1F and Supplementary Fig. 1B)**. The data suggests that the complex is composed of one TOL-1 and one LAT-1 molecule, although we cannot exclude the possibility of

lower affinity complexes that might not be observed on a size-exclusion run.

The lectin domain of LAT-1 binds to the C-LRR domain of TOL-1

To identify TOL-1- and LAT-1-binding domains, we generated a series of domain truncations of LAT-1 and TOL-1, respectively **(Fig. 2A)**. Using ECIA, we found that LAT-1 fragments comprising the whole ECD, the ECD without the GAIN domain, or the ECD without the hormone-binding and GAIN domains robustly bound to TOL-1, whereas the LAT-1 fragment without the lectin domain (comprising only the hormone-binding and GAIN domains) did not bind to TOL-1 **(Fig. 2B)**. Similarly, TOL-1 fragments comprising the whole ECD, or the ECD without the N-terminal LRR-domain robustly bound to LAT-1, whereas the TOL-1 fragment without the C-terminal LRR-domain (comprising only the N-terminal LRR domain) did not bind **(Fig. 2B)**. Western blots of the deletion constructs show that there was no significant change in the level of protein expression and secretion from the cells as compared to the wild-type protein **(Supplementary Figs. 2A,B)**. Thus, our results indicate that the lectin domain of LAT-1 and the C-terminal LRR domain of TOL-1 are required for the interaction of LAT-1 and TOL-1.

To determine whether the lectin domain of LAT-1 and the C-terminal LRR domain of TOL-1 are sufficient for the interaction of LAT-1 and TOL-1, we made baculoviruses that express only the lectin domain of LAT-1 and the C-terminal LRR domain of TOL-1 and purified them separately as recombinant proteins. The lectin domain of LAT-1 formed a stable complex with the full ECD of TOL-1 as analyzed by SEC and SDS PAGE analysis **(Fig. 2C)**. The lectin domain also formed a stable complex with the C-terminal LRR domain of TOL-1 **(Supplementary Fig. 2C)** suggesting that these domains are sufficient for the interaction of LAT-1 and TOL-1. Previous work in C. elegans showed that the Lectin domain is required for rescuing both the lethality and fertility phenotypes of *lat-1* animals.[12] Our observation that the Lectin domain is the site of TOL-1 binding is consistent with the hypothesis that the tissue

polarity and morphogenesis functions of LPHNs are mediated by interactions with TLRs.

Crystal structure of the LAT-1–TOL-1 complex reveals an unusual mode of interaction

We next set out to determine the high-resolution structure of TOL-1 in complex with LAT-1. We crystallized the full-extracellular region of TOL-1 containing both N- and C-terminal LRR domains (residues D26-S996) in a complex with the lectin domain of LAT-1 (residues T32-P136 in isoform a). We determined the x-ray structure of the complex at 4.0 Å resolution using molecular replacement **(Supplementary Table 1)**.

The crystal structure of the TOL-1/Lectin complex is a heterodimer with dimensions of ~125 Å x 45 Å x 96 Å. TOL-1 receptor is comprised of a large semicircular N-terminal LRR domain with 23 LRR repeats followed by a second but smaller C-terminal LRR domain including 5 LRR repeats **(Fig. 3A,B, and Supplementary Fig. 3A,B)**, similar to the structure of *Drosophila* Toll.[46] Each LRR domain is flanked by an N-terminal cap and a C-terminal cap **(Fig. 3A, B)**. The C-terminal LRR domain contains the LAT-1-binding site. The lectin domain of LAT-1 binds to the N-terminal cap of the C-terminal LRR domain of TOL-1 and also makes several contacts with the LRR repeats within the C-terminal LRR domain. Surprisingly, the interaction of the Lectin domain with the convex surface of the TOL-1 C-LRR domain is different from other TLR-ligand complexes, where the ligand binding site is located in the concave surface of the LRR region of most TLRs, including the DmToll and Toll5A receptors[39,40] **(Fig. 3A,B)**. The direct interaction of the TOL-1 C-terminal LRR with LAT-1 Lectin domain is consistent with our binding data and with previous studies where the lectin domain was identified as critical for the function of LAT-1 in embryo development **(Fig. 2)**. The asymmetric unit of our crystals contain four copies of the complex. The N-terminal regions of the N-terminal LRR in TOL-1 has slightly different conformations in each copy as a result of swivel-like motions, suggesting that the N-terminus of TOL-1 has intrinsic flexibility in solution **(Fig 3C)**. We observed electron density for N-linked glycosylation on TOL-1 distributed along both LRR domains, with five sites on the N-

terminal LRR domain and two additional sites on the C-terminal LRR domain.

The LAT-1 lectin domain is similar to previous lectin domain structures from other aGPCRs [24,25,41]. The LAT-1 Lectin domain adopts a kidney shaped structure with overall dimensions of 44 Å x 24 Å x 20 Å, and is composed of five β-strands and a single α-helix. A 24-residue region coming out of the lectin β-sandwich mediates the interaction with TOL-1 C-LRR **(Fig. 3A,B)**. We observed no electron density for glycosylation in the lectin domain, as predicted by sequence. **(Fig. 3D)**

Cryo-EM density of the LAT-1–TOL-1 complex agrees with the crystal structure

To verify this new mode of interaction, we also collected single-particle cryo-electron microscopy (EM) images of the full ECD TOL-1 in complex with full ECD LAT-1 and obtained a 6.3 Å density map of the full-length complex **(Fig. 4, Supplementary Fig. 4)**. 2D class averages showed a similar orientation of LAT-1 with respect to TOL-1 as observed in the crystal structure (**Fig. 4A**). Both the 2D class averages and 3D electron density maps revealed extra density at the N-terminal tip of the second LRR domain (**Fig. 4**), corresponding to the lectin domain of LAT-1. Fitting the crystal structure of the TOL-1–LAT-1 complex into the cryo-EM density map showed excellent correlation and confirmed the validity of the crystal structure (**Fig. 4B**). No density was observed for the HormR and GAIN domains of the LAT-1 molecule likely because there is a 45-amino acid linker between the Lectin and the HormR domains which is expected to introduce flexibility to the molecule. Altogether, our crystallographic structure and cryo-EM maps of the TOL-1–LAT-1 complex are in full agreement.

Structure-guided mutagenesis breaks the TOL-1–LAT-1 interaction

The TOL-1–LAT-1 interaction is mediated by an extensive combination of polar and hydrophobic residues from both proteins, creating a large buried interface area of 1412 $Å^2$ **(Fig.**

5A, B). The interface from the crystal structure is consistent with the corresponding cryo-EM electron density **(Supplementary Fig. 5)**. The TOL-1 and LAT-1 binding interface is formed by two major interaction points mediated by several interesting structural features from both proteins **(Fig. 5C)**. The loops from both TOL-1 and LAT-1 extend towards the secondary structure elements in the interacting molecule and make numerous hydrophobic and electrostatic interactions. The N-terminal cap of the C-terminal LRR domain of TOL-1 has a Cys-rich loop with six cysteines that form three disulfide bridges within the loop. These entangled disulfide bridges provide rigidity and enable extension of the loop towards LAT-1 **(Fig. 5D)**. On the LAT-1 side, a long 24-amino acid loop comes out of the β-sandwich of the lectin domain and extends towards TOL-1 **(Fig. 5E)**. A Cys-residue within this loop makes a disulfide bond with another Cys residue from the β-sandwich providing rigidity and direction to the long loop. This loop interacts with both the N-terminal cap and the leucine-rich repeats of TOL-1 C-LRR. The D79 at the tip of the long loop makes a salt bridge with the K802 on the third leucine-rich repeat of TOL-1.

To validate the binding interface, we used our crystal structure and sequence conservation analysis to design point mutations on the LAT-1-binding surface of TOL-1 and on the TOL-1-binding surface of LAT-1 that specifically disrupt the interaction. We engineered single- and multiple-point mutations on Fc-tagged TOL-1 and AP_5-tagged LAT-1, both full-length proteins, and tested the effect of the mutations on the TOL-1–LAT-1 interaction using the ECIA assay. We engineered a TOL-1 ECD mutant (Q712A-Y713A-G714A-N715A) in which we mutated four residues of a LAT-1-binding loop on TOL-1 to Ala (**Fig. 6A**). We also generated several single-site LAT-1 ECD mutants throughout the lectin domain (**Fig. 6A**). Our ECIA assay showed that TOL-1 (Q712A-Y713A-G714A-N715A) mutant has no detectable binding to wild-type LAT-1; and that the LAT-1 F69A mutant has no detectable binding to TOL-1 (**Fig. 6B**). These mutants express and are secreted from S2 cells at levels similar to the wild-type full-

length TOL-1 and LAT-1 as confirmed by western blots (Supp Figure). ECIA further confirmed that the second LRR domain of TOL-1 and Lectin domain of LAT-1 are sufficient for binding (**Fig. 6B).** These results show that our cryo-EM and crystallographic models accurately represent the complex structure and provide us with mutants that specifically break their interaction for use in functional assays.

Interaction of TOL-1 and LAT-1 is critical for embryo development and brood size in *C. elegans*.

To test whether the LAT-1–TOL-1 interaction is critical for animal development, we undertook a genome editing approach in *C. elegans*. We used CRISPR-Cas9 to generate animals with mutations in *lat-1* and *tol-1* genes designed to selectively break the LAT-1–TOL-1 interaction; we introduced the exact same mutations validated in vitro with the ECIA assay (Fig. 6). We then tested whether these engineered strains show survival and fertility phenotypes, like the ones described in *lat-1* or *tol-1 strong loss-of-function (putative* null) mutant animals. We generated two non-binding mutant strains: the *lat-1(F69A)* strain carries a single point mutation that converts F to A at position 69, whereas the *tol-1(Q712A-Y713A-G714A-N715A) strains carries four point mutations* and is referred to as *tol-1(quad mutant)*. We conducted a phenotypic analysis of these mutants (**Fig. 7A**). Intriguingly, both mutant strains, *lat-1(F69A)* and *tol-1(quad mutant)*, showed defects in brood size and embryo viability **(Fig. 7B)**. Like *tol-1* mutant animals carrying a deletion allele (nr2013), both the *tol-1(quad mutant)* and the *lat-1(F69A)* animals laid significantly fewer embryos than wildtype **(Fig. 7B)**. We also observed embryonic and larval lethality both in the *tol-1(quad mutant)* and *tol-1(nr2013)* animals, which displayed pharyngeal/anterior morphological defects **(Fig. 7C-E)**. Consistent with previous work[12], we observed that *lat-1* mutant animals carrying a deletion allele *(ok1465)* display similar anterior morphological defects **(Fig. 7F)**. These results suggest that the direct interaction of TOL-1 and

LAT-1 is critical for early development in *C. elegans*.

DISCUSSION

While many cell-surface proteins expressed in the developing embryo are known, the receptor-ligand pairings that mediate cellular interactions and regulate developmental functions remain largely enigmatic. Adhesion-GPCRs represent the second largest GPCR family in the human genome, but most adhesion-GPCRs have no known ligands, and the few that have known ligands, such as vertebrate Latrophilins, have more ligands that remain to be identified. While the interaction of vertebrate Latrophilins with TENs and FLRTs are well studied and key for their neuronal functions (ref), the ligands they interact with to execute essential functions during early embryonic development remained unclear. Several ligands were shown as Latrophilin-binding candidates, however, none of the putative *cis*- or *trans*-interacting ligands for mediating the roles of Latrophilin receptors in embryogenesis were molecularly or structurally characterized as *bona fide* physiological interactions. On the other hand, Toll receptors are a well-studied receptor family with roles in immune system in vertebrates and clear embryonic development defects in invertebrates. Here, we uncovered a convergence between the Latrophilin GPCR and the single Toll-like receptor in *C. elegans*, determined their high-resolution complex structure and revealed a functional receptor-ligand axis in embryonic development. These findings indicate that LAT-1 and TOL-1 bind directly to carry out their critical roles in *C. elegans* development and suggest possible functions for them in higher eukaryotes.

Our data afford several major conclusions. First, we discovered that LAT-1 adhesion-GPCR forms a direct complex with another signaling receptor, TOL-1 (Figures 1, 2, 3, and 4). TOL-1 is the sole Toll-like receptor in *C. elegans*. Toll-like receptors (TLRs) are critical immunological agents because of their front-line role in innate immunity against invading pathogens[1]. The signaling pathways activated by different TLRs have therefore been the focus

of much research. TLR signaling involves a family of five adaptor proteins, which couple to downstream protein kinases that ultimately lead to the activation of transcription factors such as nuclear factor-κB (NF-κB) and members of the interferon (IFN)-regulatory factor (IRF) family. The key signaling domain, which is unique to the TLR system, is the Toll/interleukin-1 (IL-1) receptor (TIR) domain, which is located in the cytosolic face of each TLR. This domain also exists in the *C. elegans* TOL-1 and is likely the domain used by TOL-1 to initiate intracellular signaling events during embryonic development.[47]

Second, The TOL-1 and LAT-1 interaction is compatible with both a *cis* and *trans* configuration. (Model **Figure 8**). Positioning the C-termini of the proteins towards the membrane and positioning the complex structure in between two neighboring cell membranes suggests that the proteins can interact in both ways. Previous studies showed that the vertebrate LPHN3 is a receptor for TEN2 in promoting synapse formation. Whether the *C. elegans* homolog of TENs, TEN-1, interacts with LAT-1 has not been tested experimentally; and based on genetic studies, this interaction may not exist in *C. elegans.* Interestingly, the Lectin domain is the binding domain for both TEN-1 and TOL-1. Superimposition of the vertebrate LPHN3–TEN2 complex structure with our invertebrate LAT-1–TOL-1 structure reveals that the Lectin domain uses a different interface for mediating these interactions. Thus, mutagenesis of the TEN-1 binding site on LAT-1 would not interfere with the interaction of LAT-1 with TEN-1 if this interaction were to exist in *C. elegans* (Supplementary Fig. 6). Of note, although Teneurin and TLR binding sites on Latrophilins are distinct and separate, a trimeric complex would not be able to form due to clashes between these two large proteins upon binding to LAT-1. An important question for future studies is whether invertebrate TEN-1 interacts with LAT-1, which could regulate the LAT-1–TOL-1 interaction.

Third, we observed that TOL-1 performs multiple, likely sequential, functions in embryonic development, which are dependent on the TOL-1–LAT-1 interaction. Using

CRISPR/Cas9 genome editing in *C. elegans*, the animals that carry point mutations in *tol-1* that abolish the interaction of TOL-1 with LAT-1 phenocopied the *tol-1* null animals, suggesting that the observed phenotypes in *tol-1* null animals are caused by the lack of interaction of TOL-1 with LAT-1 (**Fig.** 7**A–C**). On the other hand, animals that carry point mutations in *lat-1* that abolish the interaction of LAT-1 with TOL-1 phenocopied only the brood size phenotype of the *lat-1* null animals suggesting that not all phenotypes observed for the *lat-1* null animals are caused by the lack of the LAT-1 -TOL-1 interaction (Fig. 7).

Finally, our study poses the question of whether Latrophilin-TLR interactions are present in other taxa, especially in flies and vertebrates. In humans, there are three Latrophilins and 10 TLRs, and it is possible that specific sets of human LPHNs and TLRs may interact. It is also possible that the *Drosophila* Latrophilin*,* Cirl, not only interacts with Toll-8 (Tollo), as it was very recently proposed by Lavalou et al.,[39] but also with other paralogs among the nine-member fly TLR family. This has the potential to find novel functions for a Latrophilin-TLR interaction in other model organisms.

In summary, our data suggest that the direct interaction of the extracellular regions of LAT-1 and TOL-1 is key for embryo development in *C. elegans*, and its absence leads to partial sterility, lethality, and malformed embryos. They likely exert these functions through *trans*-cellular interactions which may activate downstream signaling pathways of LAT-1 and TOL-1. These inter interactions involve an unexpected atomic mechanism that requires a highly specific set of binding modules , previously not observed in ligand-receptor interactions. Since there are three LPHNs, 10 TLRs and numerous LRR repeat containing homologous proteins in mammals, it seems likely that the *trans*-cellular regulatory mechanisms critical for early embryo development observed here may broadly apply to other organisms. This work provides the foundation to reveal new axes of cellular signaling and coordination between two signaling receptor families in the developing embryo, pioneering the identification of homologous pathways in mammals.

Figure Legends

Figure 1. LAT-1 binds to TOL-1 with high affinity

(A) Domain architecture schematics of LAT-1, the *C. elegans* homolog of Latrophilin.

(C, D) *Z*-scores for AP signal observed against a LAT-1-Fc bait (B) and TOL-1-Fc bait (C). Highest signals are observed for AP-tagged TOL-1 (B) and LAT-1 (C).

(B) Domain architecture schematics of TOL-1, the only *C. elegans* homolog of Toll-like receptors.

(E) SEC profiles of full ECDs of TOL-1, LAT-1 and their complex; and the SDS-PAGE analysis of the fractions form the complex peak. Numbers indicate the collected fractions.

(F) MALS analysis of the complex peak showing a molecular weight of 172 kDa corresponding to a 1:1 stable complex of TOL-1 (112.1 kDa) and LAT-1 (58.9 kDa) which adds up to 171 kDa). Also see Supplementary Fig. 1.

Figure 2. The Lectin domain of LAT-1 and the C-terminal LRR of TOL-1 mediate the LAT-1 –TOL-1 interaction.

(A) Schematic of LAT-1 and TOL-1 domain structures and the domain deletion constructs used to map the domains involved in binding.

(B) Mapping interacting domains in the LAT-1–TOL-1 complex using ECIA. TOL-1-Fc bait were used to capture LAT-1-AP prey. Binding was detected by absorbance at 650 nm, corresponding to the absorbance of the AP product. Also see Supplementary Fig. 2.

(C) The LAT-1 Lectin domain forms a stable complex with the full-length ECD of TOL-1 as shown by SEC profiles and SDS-PAGE analysis of the complex fractions.

Figure 3. Crystal structure of the LAT-1–TOL-1 complex reveals a previously unobserved mode of interaction

(A, B) Crystal structure of the complex of TOL-1 ECD (cyan) with the LAT-1 Lectin domain (pink) (A, cartoon view; B, surface view).

(C) Superimposition of the four symmetry elements in the asymmetric unit showing the flexibility of the N-terminal tip of TOL-1.

(D) The interacting surfaces in the TOL-1–LAT-1 Lectin complex are highly conserved. Coloring reflects conservation between 150 sequences from invertebrates. Also see Supplementary Fig. 3.

Figure 4. Single-particle cryo-EM density of the full-ECD LAT-1–TOL-1 complex at 6.3 Å resolution.

(A) 2-D cryo-EM averages of the TOL-1 ECD–LAT-1 ECD complex. The additional density corresponding to the Lectin domain of LAT-1 is indicated by a yellow circle. The rest of LAT-1 is not visible in averages.

(B) 3-D map reconstruction of the TOL-1 ECD–LAT-1 ECD complex with the higher-resolution crystal structure of the complex fit into the cryo-EM density. Also see Supplementary Fig. 4.

Figure 5. The binding Interface of the LAT-1–TOL-1 complex is large and is mediated by large loops.

(A) The structure of the LAT-1–TOL-1 complex binding interface is shown using a cartoon representation, with only the domains involved in the interface used. Disulfide bonds are shown by yellow sticks.

(B) (Left) Same as in A but in in surface representation. (Right) Illustrates the buried surfaces using an open book view. Light pink and light blue colors are used to highlight portions of the surfaces involved in the interface.

(C) A zoomed in view of the interface in A with side chains shown as sticks. The surface is broadly divided into two patches, each highlighted with a colored oval.

(D, E) patches 1, and 2 are shown in detail, with individual residues shown as sticks, with salt bridges and hydrogen bonds shown in yellow dotted lines. See also Supplementary Fig. 5.

Figure 6. Structure-guided point mutations disrupt the interaction of the LAT-1 and TOL-1.

(A) The LAT-1 and TOL-1 interface is shown in a cartoon representation, with key side chains shown as sticks and labeled.

(B) ECIA results show that LAT-1 mutations at the TOL-1 interface can diminish or abolish TOL-1 binding. A quadruple TOL-1 mutant designed at the interface also abolishes LAT-1 binding. Also see Supplementary Fig. 2.

Fig. 7. Interaction of TOL-1 and LAT-1 is critical for embryo development and brood size in *C. elegans*.

(A) Experimental design for testing the brood size and lethality phenotypes for the engineered *lat-1* and *tol-1* binding mutants.

(B) Phenotypes comparing WT, null *tol-1(nr2013)*, *tol-1(quad mut)*, null *lat-1(ok1465)* and *lat-1(F69A)* animals. For brood size (left), data shown are the number of embryos lain per plated L4 animal over the course of 24 hours; For embryonic survival (center), data shown are percentages of embryos that hatch within 24 hours of being lain; for larval survival (right), data shown are percentages of larvae that hatch and survive to adulthood within 94 hours of being lain. Statistical comparisons for brood size, embryonic lethality, and larval lethality of wildtype and each mutant were conducted using a one-tailed t-test (p-value < 0.01 are considered significant); exact p-values are displayed above each individual comparison; p-values in black

are significant, whereas *p*-values in grey are not. Error bars refer to the standard error of the mean (SEM).

(C) Representative DIC images of wildtype (N2) animals at early, mid, and late stages of embryogenesis (top) and during the first larval stage (L1, bottom).

(D-E) Representative DIC images of morphological phenotypes observed in *tol-1(nr2013)* null and *tol-1(quad mutant)* embryos (top) and L1 larvae (bottom). Yellow lines trace the pharyngeal boundaries.

(F) Representative DIC-Fluorescence micrograph overlay of heterozygous/balanced *lat-1* L1 larva, labeled with pharyngeal GFP (left) and representative DIC images of morphological phenotypes observed in null *lat-1(ok1465)* embryos (top right) and larvae (bottom right).

Fig 8. Model showing the interaction of LAT-1 and TOL-1 is important for embryo development

The LAT-1–TOL-1 complex identified in this work is compatible with both a *trans* interaction mode, A, and a *cis* interaction mode, B. Each interaction mode may lead to key functions of both LAT-1 and TOL-1 in embryo development.

(A) The *trans* interaction mode is the more likely mode for the LAT-1 and TOL-1 interaction. The intracellular TIR domain of TOL-1 and the intracellular G-protein coupling of LAT-1 might be involved in intracellular signal transduction into the developing embryo. Two opposing cell membranes are shown with LAT-1 and TOL-1 molecules projecting out of them, with intracellular faces towards the top and bottom of the page, and an extracellular space in the middle of the page. LAT-1 and TOL-1 are shown as a cartoon representation, linked to their transmembrane helices (shown as rounded cylinders).

(B) The *cis* interaction mode is less likely but possible. It might also have a role in regulating the occurrence of the *trans*-interaction to control biological function.

METHODS

Cell culture:

High-Five insect cells (*Trichoplusia ni*, female, ovarian. Thermo Fisher, B85502) cultured in Insect-Xpress medium (Lonza, 04351Q) supplemented with 10 µg/mL gentamicin at 27°C were used for production of recombinant proteins. HEK293 and HEK293T mammalian cells (ATCC, CRL-3216) were used for cell-surface expression, flow cytometry, SRE, cAMP signaling and cell aggregation assays and were cultured in Dulbecco's modified Eagle's medium (DMEM; Gibco, 11965092) supplemented with 10% FBS (Sigma-Aldrich, F0926) at 37°C in 5% CO_2.

Cloning and expression in insect cells:

Caenorhabditis elegans TOL-1 (Uniprot Q9N5Z3_CAEEL) and LAT-1 (Lat1, Uniprot LPLT1_CAEEL) constructs were cloned into a pAcGP67a vector and expressed in High-Five insect cells using the baculovirus expression system. Sf9 cells (Thermo Fischer, 12659017) were co-transfected with the linearized baculovirus DNA (Expression Systems, 91-002) and the constructed plasmid using the Cellfectin II (Thermo Fischer, 10362100) transfection reagent. Baculovirus was amplified in Sf9 cells in SF900-III medium containing 10% (v/v) FBS (Sigma-Aldrich, F0926). Large-scale protein expression was performed by infection of High-Five cells (Thermo Fisher, B85502) in Insect-Xpress medium (Lonza, 12-730Q) at a cell density of 2.0 x 10^6 cells/ml for 72 hours at 27°C.

For the structural studies, TOL-1 ECR (residues D26-S996), LAT-1 ECR (residues S28-T552) and LAT-1 Lec domain (residues T32-P136) were cloned with carboxyl-terminal 6X His-tags separately and co-expressed in High-Five insect cells. The following primers were used for amplification of High Five cells expressed *C. elegans* Tol1 ECR: TOL-1: F: 5'-TGGCATGAAGCGGATCCCGGGTACACCGATGAGTGCCCCAAGTTC-3', and R: 3'-GCGGCCGCTCCGGAATTCTAGTTAGTGCTGGATATCGCTGTTCTGTGG-5'. The following primers were used for amplification of High Five cells expressed *C. elegans* LAT-1 ECR: LAT-1: F: 5'- CATTCTGCCTTTGCGGCGGTACCCAGCAACAAGCCGACA-3', and R: 3'-

GTTCTTGCCGGGTCCCAGTTAGTGGTGATGGTGATGATGAGTGAGAAGCGTTTGGTC-5'.

The following primers were used for amplification of High Five cells expressed in LAT-1 Lec domain: LAT-1 Lec: F: 5'-TGCCTTTGCGGCGGATCCcACAACGGATGAAAGTGGA-3', and R: 3'-AAGGATCAGATCTGCAGCTTAATGATGATGATGATGATGAGGAACAACACAATTGTA-5'.

72 hours after transfection, the medium containing secreted glycosylated proteins was collected and centrifuged at 900 x *g* for 15 minutes at a room temperature. The supernatant was transferred into a baker and mixed with (final concentration): 50 mM Tris pH 8.0, 5 mM $CaCl_2$ and 1 mM $NiCl_2$ and stirred for 30 minutes. After centrifugation at 8000 g for 30 minutes, the clarified supernatant was incubated with nickel-nitrilotriacetic agarose resin (QIAGEN) for 3 hours at room temperature. The resin was collected with a glass Buchner funnel and rinsed with HBS buffer containing 20 mM imidazole, then transferred to a poly-prep chromatography column (Bio-rad). The protein was eluted with HBS buffer containing 200 mM imidazole and run on size-exclusion chromatography (Superdex 200 10/300 GL; Superose 6 Increase 10/300 columns; GE Healthcare), purified in a final buffer comprised of 10 mM Tris pH 8.5, 150 mM NaCl. For the flow cytometry binding assays, LAT-1 Lec (residues T32-P136) was cloned with carboxyl-terminal 6X His-AVI tags and captured on nickel-nitrilotriacetic resin as described above. The following primers were used for amplification of High Five cells expressed *C. elegans* LAT-1 Lec-Avi-Tag: LAT-1 Lec-AVI: F: 5'-GGCGGCGGCGCATTCTGCCTTTGCGGCGACAACGGATGAAAGTGGAA-3', and R: 5'-AGCCTCGAAAATATCATTAAGACCGCGAGGAACAACACAATTGTATTTCACTTCCAG-3'

Following a wash with HBS buffer containing 20 mM imidazole, final concentration of 50 mM Bicine pH 8.3, 100 mM NaCl, 100 mM Mg-acetate, 10 mM ATP, 0.5 mM biotin and 5 mM BirA were added to the resin, which was then rotated for 2 hours at 27 °C. After removing residual BirA and ATP by washing with HBS buffer containing 20 mM imidazole, the biotinylated lectin was eluted with HBS buffer containing 200 mM imidazole. Purified protein was applied to size-

exclusion chromatography. The efficiency of biotinylation was assed using streptavidin bead pulldown assay.

The extracellular interactome assay (ECIA):

The ectodomain of TOL-1 and LAT-1 were cloned into the pCE217-bait (TOL-1-Fc-tagged) and pCE176-prey (LAT-1-AP-tagged) plasmids, respectively, and expressed in Schneider S2 cells. The following primers were used for amplification of S2 cells expressed *C. elegans* TOL-1-Fc-tagged: TOL-1-Fc: F: 5'-CCTCGCTCGGGGAGGTACCG-3', and R: 3'-CTCCGCCACTGTGCTGGATATCG-5'. The following primers were used for amplification of S2 cells expressed *C. elegans* LAT-1-AP-tagged: LAT-1-AP: F: 5'-CCTCGCTCGGGGAGGTACCCA-3', and R: 3'-TCCGCCACTGTGCTGGATATCAGTGAGAA-5'. The assay was performed as described before (ref). When mutants of TOL-1 and LAT-1 constructs were tested for binding, the expression levels of the bait and prey were normalized for comparison purposes by quantitation via western blot.

Quantitation by Western Blot:

Quantitation of TOL-1-Fc-tagged and LAT-1-AP-tagged secreted proteins in conditioned media for ECIA was performed using western blots against the hexahistidine tag present at the C-termini of all constructs (antibody: fluorescent His-Tag Antibody with iFlour 488, Genscript, catalog no. A01800, 1:500 dilution). Quantitation of fluorescent signal was performed using a Biorad Chemidoc system and ImageLab version 6 (Biorad).

Multi-angle Light Scattering (MALS):

MALS experiments were done on a Wyatt HELEOS II scattering detector coupled to an AKTA FPLC (GE Healthcare) with a Superose 6 Increase 10/300 column using HBS as the sample and running buffer. For data collection and analysis, ASTRA software version 5.3.4 (Wyatt Technology Corp) was used. Average molar mass values calculated using the Zimm model were 169 kDa for the TOL-1/Lec complex (expected heterodimer: 171 kDa).

X-ray crystallography:

Initial screens for crystallization of the TOL-1/Lec complex were carried out using 96-well format kits (NeXtal Biotech) on a Crystal Gryphon crystallization robot (Art Robbins Instruments). Automatic plate scanning by a Rock Imager imaging system (Formulatrix) identified initial hits. After multiple rounds of optimization, crystals of TOL-1/Lec were grown using hanging-drop vapor diffusion at 16 mg mL-1 in 0.2 M Sodium Malonate, 0.1 M Bis-Tris-Propane pH 4.5, 26% PEG 3350, 1.2% Myo-Inositol. Crystals grew to full size within 4 weeks. Crystals were cryoprotected by transferring the crystals into mother liquor with 10, 15, and 20% of glycerol gradually. Data were collected to 4.2 Å at the Advanced Photon Source at Argonne National Laboratory (beamline XX-XX-XX).

Cryo-EM data acquisition:

3.5 µl purified TOL-1/Lec complex (0.28 mg/ml) was applied on glow-discharged holey carbon grids (Quantifoil R1.2/1.3, 200 mesh), and vitrified using a Vitrobot Mark IV (FEI Company). The specimen was visualized using Titan Krios electron microscope (FEI) operating at 300kV and equipped with a K3 direct electron detector (Gatan, Inc.). Images were recorded with a nominal magnification of x81,000 in super-resolution counting mode, corresponding to a pixel size of 0.5315 Å on the specimen level. To maximize data collection speed while keeping image aberrations minimal, image shift was used as imaging strategy using one data position per hole with four holes targeted in one template with one focus position. In total, 3333 images with defocus values in the range of -1.0 to -2.5 µm were recorded using a dose rate of 14.6 electrons/$Å^2$/s. The total exposure time was set to 4.2 s with frames recorded every 0.105 s, resulting in an accumulated dose of about 60.1 electrons per $Å^2$ and a total of 40 frames per movie stack.

Image processing and 3D reconstruction:

Stack images were subjected to beam-induced motion correction using MotionCor. CTF parameters for each micrograph were determined by CTFFIND4. In total, 1,492,070 particle

projections were selected using automated particle picking and subjected to reference-free two-dimensional classification to discard false-positive particles or particles categorized in poorly defined classes, resulting in 1,346,788 particle projections for further processing. Three-dimensional classifications were initially performed on a binned dataset with a pixel size of 2.126 Å using RELION-3. An ab initio 3D map generated in RELION was used as initial reference model for the first round of maximum-likelihood-based 3D classification. 3D refinement and post-processing was performed on the best class with clear features. The detailed data processing flow is shown in Supplementary Fig 4. Reported resolutions are based on the gold-standard Fourier shell correlation (FSC) using the 0.143 criterion (Supplementary Fig. 4B).

Cloning and expression in mammalian cells:

Full length TOL-1 (residues D26-V1221) LAT-1 (residues M1-L1014) and TEN (residues M1-E2693) constructs bearing N-terminal FLAG-tags were cloned into a pcDNA3.1 vector for cell-surface expression and flow cytometry binding assays in HEK293T cells. The following primers were used for amplification of HEK cells expressed TOL-1 FL: TOL-1 FL: F: 5'-GACGATGACGATAAATTTGATGAGTGCCCCAAGTTCTGC-3', and R: 5'-TGTGCTGGATATCTGCAGAATTCCTAAACAACATCGGAAGGCACAA-3'. The following primers were used for amplification of HEK cells expressed LAT-1 FL: LAT-1 FL: F: 5'-GACGATGACGATAAATTTATGCGACGTAACAAAACGACTTATTC-3', and LAT-1 FL: R: 3'-ACTGTGCTGGATATCTGCAGAATTCCTATAAATCTTGACAATACATGCTCGGCT-5'. The following primers were used for amplification of HEK cells expressed Ten FL: XXXXXXXXX and, XXXXXXXXXXXXXX. TOL-1 FL mutant was generated using a standard two-step PCR-based strategy with the internal primers: TOL-1 QYGN/A: TOL-1 QYGN/A F: 5'-CCGGAGTGCATCTGCTGCGCGGCCGCCGCTTGCGACTGCAAGTCGGTG-3', and TOL-1 QYGN/A: R: 3'-CGCAAGCGGCGGCCGCGCAGCAGATGCACTCCGGCTC-5'. LAT-1 FL mutant was generated using a standard two-step PCR-based strategy with the internal primers:

LAT-1 F69A: F: 5'-CTAGGAAACTATGGAAGAGCATCTGTCGCTGTTTGCCTT-3', and R: 3'-AAGGCAAACAGCGACAGATGCTCTTCCATAGTTTCCTAG-5'. TEN FL mutant was generated using a standard two-step PCR-based strategy with internal primers

***C. elegans* Brood size and viability assays**

Four to five L4 stage-matched hermaphrodite larvae of each genotype were placed on separate 35 mm plates spotted with OP50 or *E. coli* HT115[DE3]. Hermaphrodites were allowed to lay embryos at 25°C for 24 hours. After the 24-hour period, adult worms were removed from plates and total progeny were counted and divided by the number of L4 hermaphrodites originally plated to arrive at brood size number. Progeny at 24 hours were also scored into 2 categories: embryos or larvae. Embryonic survival is expressed as a percentage and was calculated as the number of hatched larvae at 48 hours divided by the total number of embryos laid at 24 hours. Larval survival is expressed as a percentage and was calculated as the number of adults counted at 96 hours divided by the total number of hatched larvae counted at 48 hrs.

***C. elegans* Microscopy.** Larval animals were anesthetized with sodium azide (NaN_3, 100 mM). Embryonic or larval stage animals were mounted on a 4% agarose pad on imaging slides. Differential interference contrast (DIC) and fluorescent images were taken on an automated fluorescence microscope (Zeiss, Axio Imager Z2) using a Zeiss Axiocam 503 mono (ZEN Blue software, version 2.3.69.1000) equipped with a 63x oil immersion objective. Representative images shown are single z slices. Image reconstruction was performed in Fiji (version 2.9.0/1.53t). Fluorescent overlay and image cropping for figure 5 was performed using Adobe Photoshop and Illustrator (23.2.2 Release)

References

1. Basson, M. A. Signaling in cell differentiation and morphogenesis. *Cold Spring Harb. Perspect. Biol.* **4**, a008151 (2012).
2. Schöneberg, T. & Prömel, S. Latrophilins and Teneurins in Invertebrates: No Love for Each Other? *Front. Neurosci.* **13**, 154 (2019).
3. Topf, U. & Drabikowski, K. Ancient Function of Teneurins in Tissue Organization and Neuronal Guidance in the Nematode Caenorhabditis elegans. *Front. Neurosci.* **13**, 205 (2019).
4. Krasnoperov, V. G. *et al.* alpha-Latrotoxin stimulates exocytosis by the interaction with a neuronal G-protein-coupled receptor. *Neuron* **18**, 925–937 (1997).
5. Lelianova, V. G. *et al.* Alpha-latrotoxin receptor, latrophilin, is a novel member of the secretin family of G protein-coupled receptors. *J. Biol. Chem.* **272**, 21504–21508 (1997).
6. Sugita, S., Khvochtev, M. & Südhof, T. C. Neurexins are functional alpha-latrotoxin receptors. *Neuron* **22**, 489–496 (1999).
7. Südhof, T. C. alpha-Latrotoxin and its receptors: neurexins and CIRL/latrophilins. *Annu. Rev. Neurosci.* **24**, 933–962 (2001).
8. Schiöth, H. B., Nordström, K. J. V. & Fredriksson, R. The adhesion GPCRs; gene repertoire, phylogeny and evolution. *Adv. Exp. Med. Biol.* **706**, 1–13 (2010).
9. Hayflick, J. S. A family of heptahelical receptors with adhesion-like domains: a marriage between two super families. *J. Recept. Signal Transduct. Res.* **20**, 119–131 (2000).
10. Araç, D. *et al.* A novel evolutionarily conserved domain of cell-adhesion GPCRs mediates autoproteolysis. *EMBO J.* **31**, 1364–1378 (2012).
11. Moreno-Salinas, A. L. *et al.* Latrophilins: A Neuro-Centric View of an Evolutionary Conserved Adhesion G Protein-Coupled Receptor Subfamily. *Front. Neurosci.* **13**, 700 (2019).
12. Langenhan, T. *et al.* Latrophilin signaling links anterior-posterior tissue polarity and oriented cell divisions in the C. elegans embryo. *Dev. Cell* **17**, 494–504 (2009).
13. Prömel, S. *et al.* The GPS motif is a molecular switch for bimodal activities of adhesion class G protein-coupled receptors. *Cell Rep.* **2**, 321–331 (2012).
14. Silva, J.-P. & Ushkaryov, Y. A. The latrophilins, ‘split-personality’ receptors. *Adv. Exp. Med. Biol.* **706**, 59–75 (2010).
15. Vitobello, A. *et al.* ADGRL1 haploinsufficiency causes a variable spectrum of neurodevelopmental disorders in humans and alters synaptic activity and behavior in a

mouse model. *Am. J. Hum. Genet.* **109**, 1436–1457 (2022).

16. Anderson, G. R. *et al.* Postsynaptic adhesion GPCR latrophilin-2 mediates target recognition in entorhinal-hippocampal synapse assembly. *J. Cell Biol.* **216**, 3831–3846 (2017).
17. Lee, C.-S. *et al.* The G Protein-Coupled Receptor Latrophilin-2, A Marker for Heart Development, Induces Myocardial Repair After Infarction. *Stem Cells Transl. Med.* **11**, 332–342 (2022).
18. Röthe, J. *et al.* Involvement of the Adhesion GPCRs Latrophilins in the Regulation of Insulin Release. *Cell Rep.* **26**, 1573-1584.e5 (2019).
19. Kocibalova, Z. *et al.* Development of Multidrug Resistance in Acute Myeloid Leukemia Is Associated with Alterations of the LPHN1/GAL-9/TIM-3 Signaling Pathway. *Cancers* **13**, 3629 (2021).
20. Camillo, C. *et al.* LPHN2 inhibits vascular permeability by differential control of endothelial cell adhesion. *J. Cell Biol.* **220**, e202006033 (2021).
21. Lee, C.-S. *et al.* Adhesion GPCR Latrophilin-2 Specifies Cardiac Lineage Commitment through CDK5, Src, and P38MAPK. *Stem Cell Rep.* **16**, 868–882 (2021).
22. Bucar, E. B., Carmelo, A., Thai, M. H. & Frey, M. R. Loss of Adhesion G-Protein-Coupled Receptor L2 Expression Impacts Colonic Epithelial Proliferation. *FASEB J.* **36**, (2022).
23. Arcos-Burgos, M. *et al.* A common variant of the latrophilin 3 gene, LPHN3, confers susceptibility to ADHD and predicts effectiveness of stimulant medication. *Mol. Psychiatry* **15**, 1053–1066 (2010).
24. O'Hayre, M. *et al.* The emerging mutational landscape of G proteins and G-protein-coupled receptors in cancer. *Nat. Rev. Cancer* **13**, 412–424 (2013).
25. Kan, Z. *et al.* Diverse somatic mutation patterns and pathway alterations in human cancers. *Nature* **466**, 869–873 (2010).
26. Sumbayev, V. V. *et al.* Expression of functional neuronal receptor latrophilin 1 in human acute myeloid leukaemia cells. *Oncotarget* **7**, 45575–45583 (2016).
27. Meza-Aguilar, D. G. & Boucard, A. A. Latrophilins updated. *Biomol. Concepts* **5**, 457–478 (2014).
28. Silva, J.-P. *et al.* Latrophilin 1 and its endogenous ligand Lasso/teneurin-2 form a high-affinity transsynaptic receptor pair with signaling capabilities. *Proc. Natl. Acad. Sci. U. S. A.* **108**, 12113–12118 (2011).
29. Sugita, S., Ichtchenko, K., Khvotchev, M. & Südhof, T. C. alpha-Latrotoxin receptor CIRL/latrophilin 1 (CL1) defines an unusual family of ubiquitous G-protein-linked receptors.

G-protein coupling not required for triggering exocytosis. *J. Biol. Chem.* **273**, 32715–32724 (1998).

30. Li, J. *et al.* Alternative splicing controls teneurin-latrophilin interaction and synapse specificity by a shape-shifting mechanism. *Nat. Commun.* **11**, 2140 (2020).
31. del Toro, D. *et al.* Structural Basis of Teneurin-Latrophilin Interaction in Repulsive Guidance of Migrating Neurons. *Cell* **180**, 323-339.e19 (2020).
32. Nazarko, O. *et al.* A Comprehensive Mutagenesis Screen of the Adhesion GPCR Latrophilin-1/ADGRL1. *iScience* **3**, 264–278 (2018).
33. Sando, R., Jiang, X. & Südhof, T. C. Latrophilin GPCRs direct synapse specificity by coincident binding of FLRTs and teneurins. *Science* **363**, eaav7969 (2019).
34. Zhang, R. S., Liakath-Ali, K. & Südhof, T. C. Latrophilin-2 and latrophilin-3 are redundantly essential for parallel-fiber synapse function in cerebellum. *eLife* **9**, e54443 (2020).
35. Boucard, A. A., Maxeiner, S. & Südhof, T. C. Latrophilins function as heterophilic cell-adhesion molecules by binding to teneurins: regulation by alternative splicing. *J. Biol. Chem.* **289**, 387–402 (2014).
36. Li, J. *et al.* Structural Basis for Teneurin Function in Circuit-Wiring: A Toxin Motif at the Synapse. *Cell* **173**, 735-748.e15 (2018).
37. O'Sullivan, M. L. *et al.* FLRT proteins are endogenous latrophilin ligands and regulate excitatory synapse development. *Neuron* **73**, 903–910 (2012).
38. Lu, Y. C. *et al.* Structural Basis of Latrophilin-FLRT-UNC5 Interaction in Cell Adhesion. *Struct. Lond. Engl. 1993* **23**, 1678–1691 (2015).
39. Lavalou, J. *et al.* Formation of polarized contractile interfaces by self-organized Toll-8/Cirl GPCR asymmetry. *Dev. Cell* **56**, 1574-1588.e7 (2021).
40. Bushell, K. M., Söllner, C., Schuster-Boeckler, B., Bateman, A. & Wright, G. J. Large-scale screening for novel low-affinity extracellular protein interactions. *Genome Res.* **18**, 622–630 (2008).
41. Özkan, E. *et al.* An Extracellular Interactome of Immunoglobulin and LRR Proteins Reveals Receptor-Ligand Networks. *Cell* **154**, 228–239 (2013).
42. Wojtowicz, W. M. *et al.* A vast repertoire of Dscam binding specificities arises from modular interactions of variable Ig domains. *Cell* **130**, 1134–1145 (2007).
43. Voulgaraki, D. *et al.* Multivalent recombinant proteins for probing functions of leucocyte surface proteins such as the CD200 receptor. *Immunology* **115**, 337–346 (2005).
44. Botos, I., Segal, D. M. & Davies, D. R. The structural biology of Toll-like receptors. *Struct. Lond. Engl. 1993* **19**, 447–459 (2011).

45. Pujol, N. *et al.* A reverse genetic analysis of components of the Toll signaling pathway in Caenorhabditis elegans. *Curr. Biol. CB* **11**, 809–821 (2001).
46. Parthier, C. *et al.* Structure of the Toll-Spatzle complex, a molecular hub in Drosophila development and innate immunity. *Proc. Natl. Acad. Sci. U. S. A.* **111**, 6281–6286 (2014).
47. O'Neill, L. A. J. & Bowie, A. G. The family of five: TIR-domain-containing adaptors in Toll-like receptor signalling. *Nat. Rev. Immunol.* **7**, 353–364 (2007).
48. Scholz, N. *et al.* Molecular sensing of mechano- and ligand-dependent adhesion GPCR dissociation. *Nature* **615**, 945–953 (2023).
49. Fitzgerald, K. A. & Kagan, J. C. Toll-like Receptors and the Control of Immunity. *Cell* **180**, 1044–1066 (2020).
50. Drabikowski, K., Trzebiatowska, A. & Chiquet-Ehrismann, R. ten-1, an essential gene for germ cell development, epidermal morphogenesis, gonad migration, and neuronal pathfinding in Caenorhabditis elegans. *Dev. Biol.* **282**, 27–38 (2005).

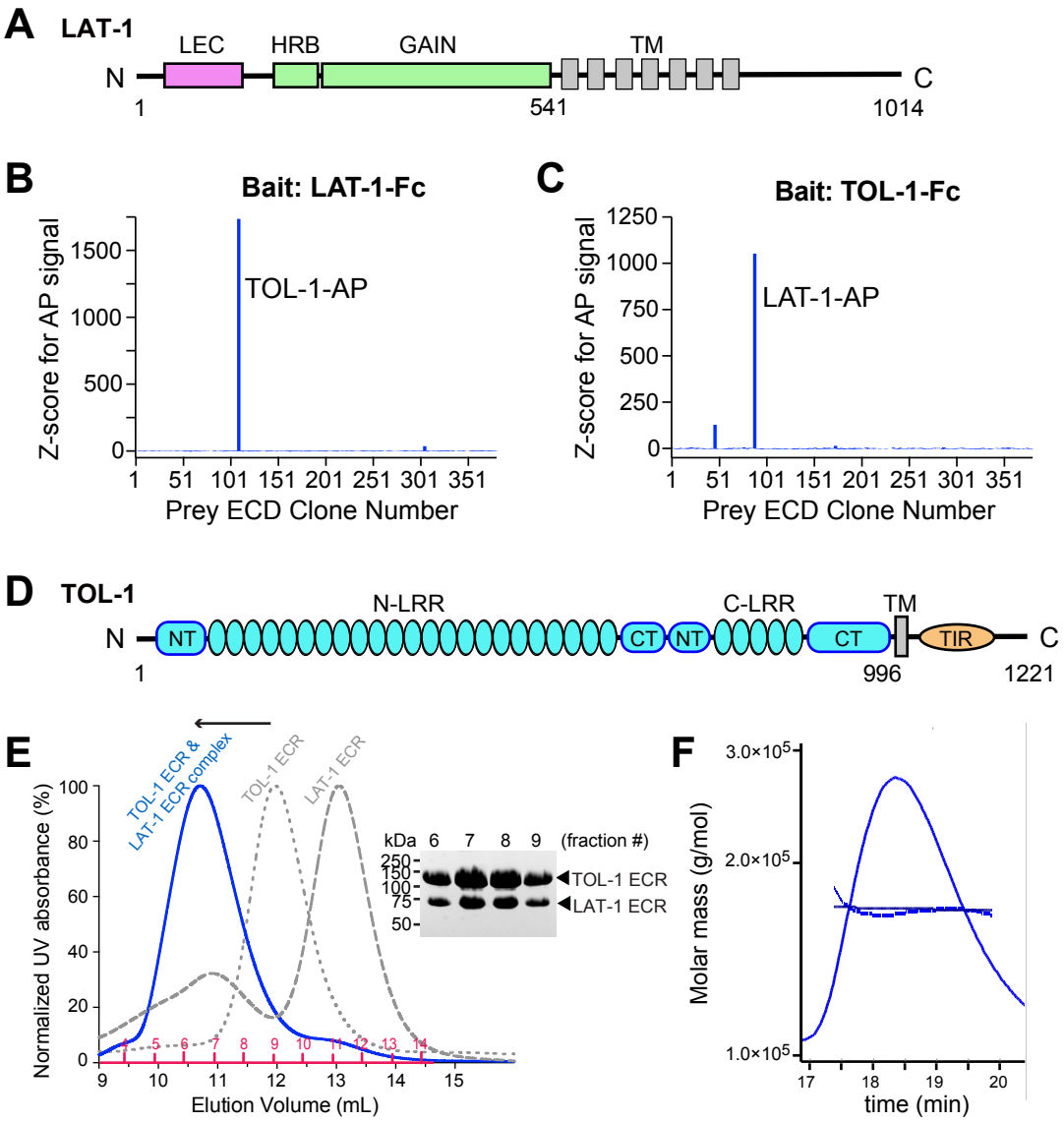

Carmona-Rosas et al., Figure 1

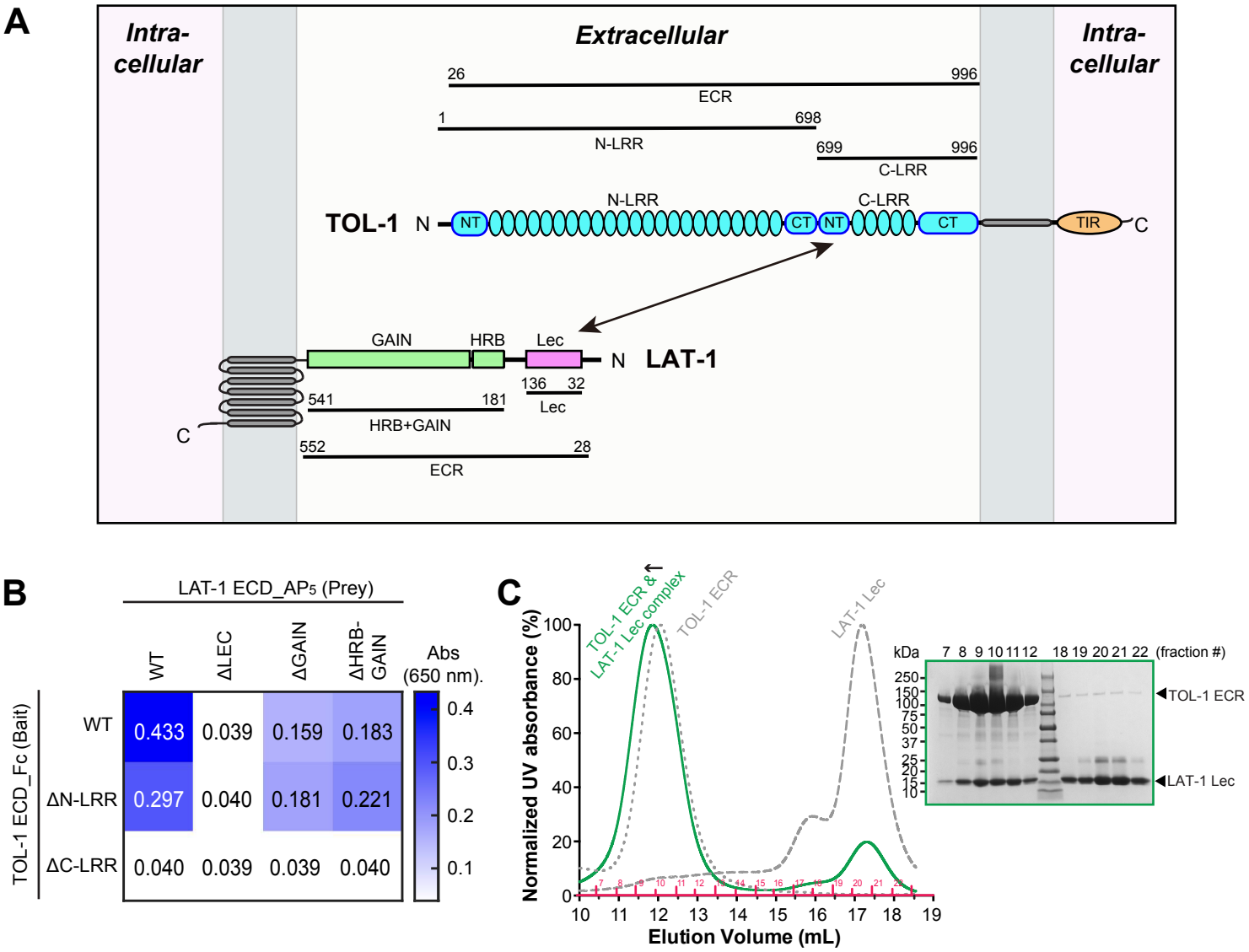

Carmona-Rosas et al., Figure 2

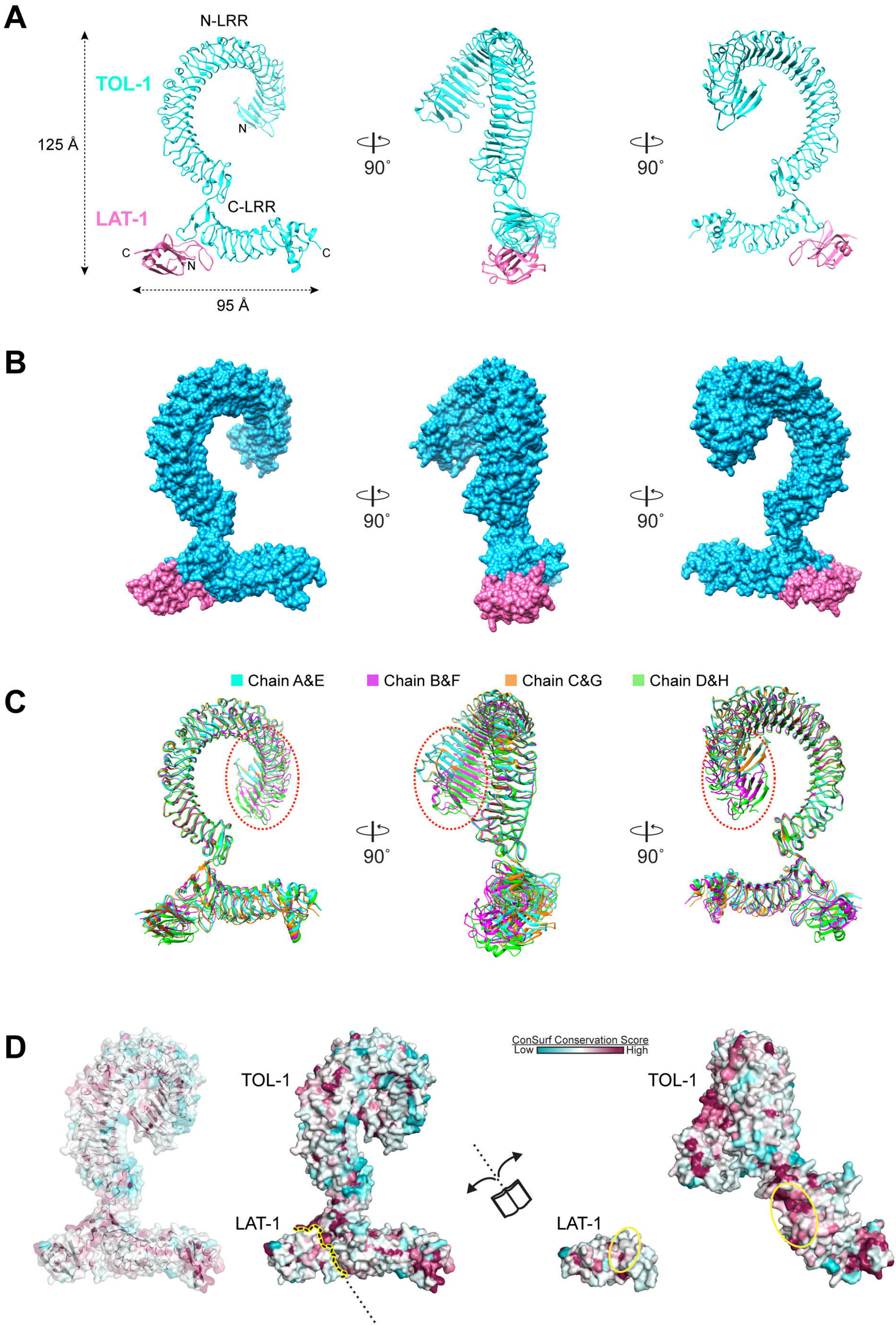

Carmona-Rosas et al., Figure 3

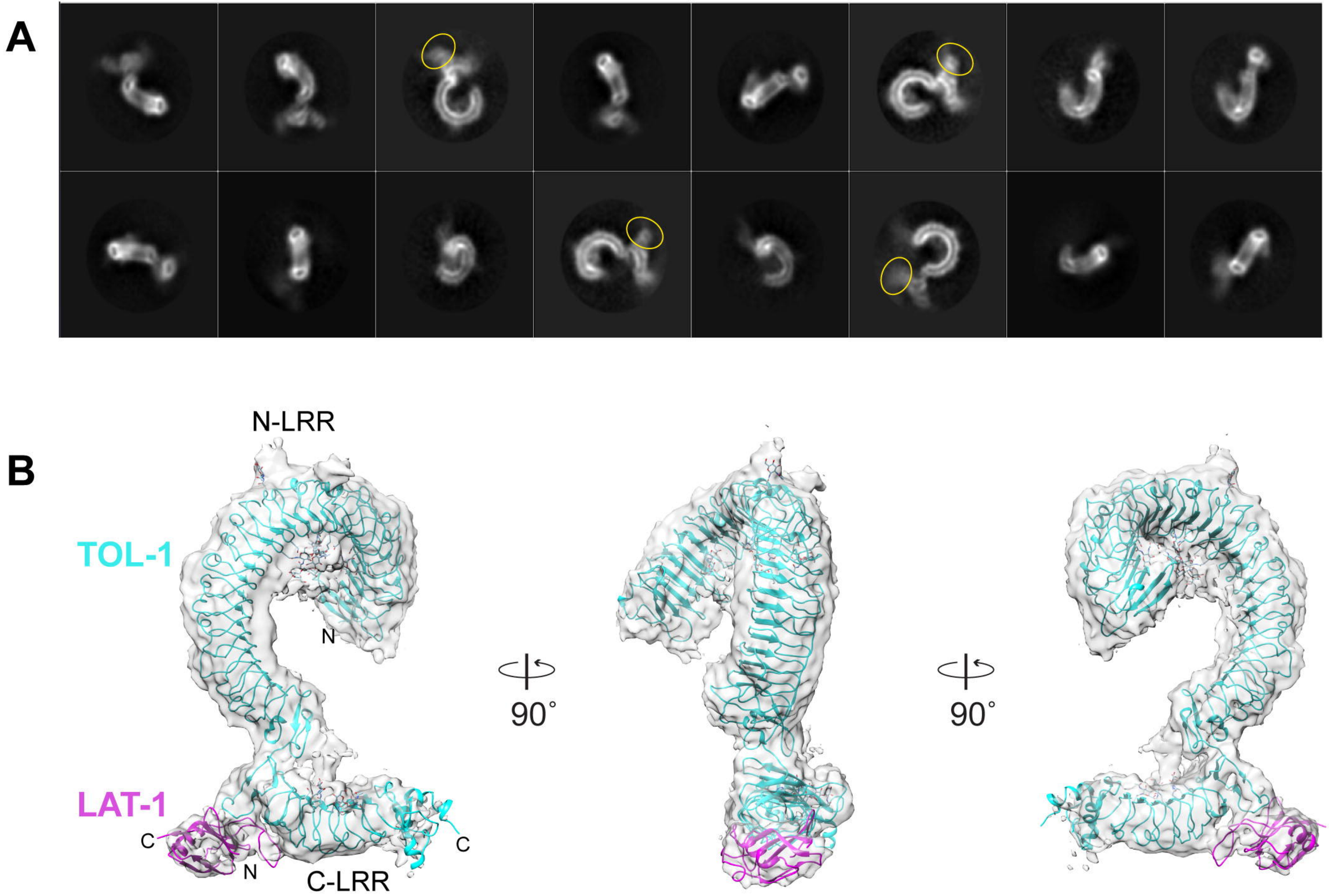

Carmona-Rosas et al., Figure 4

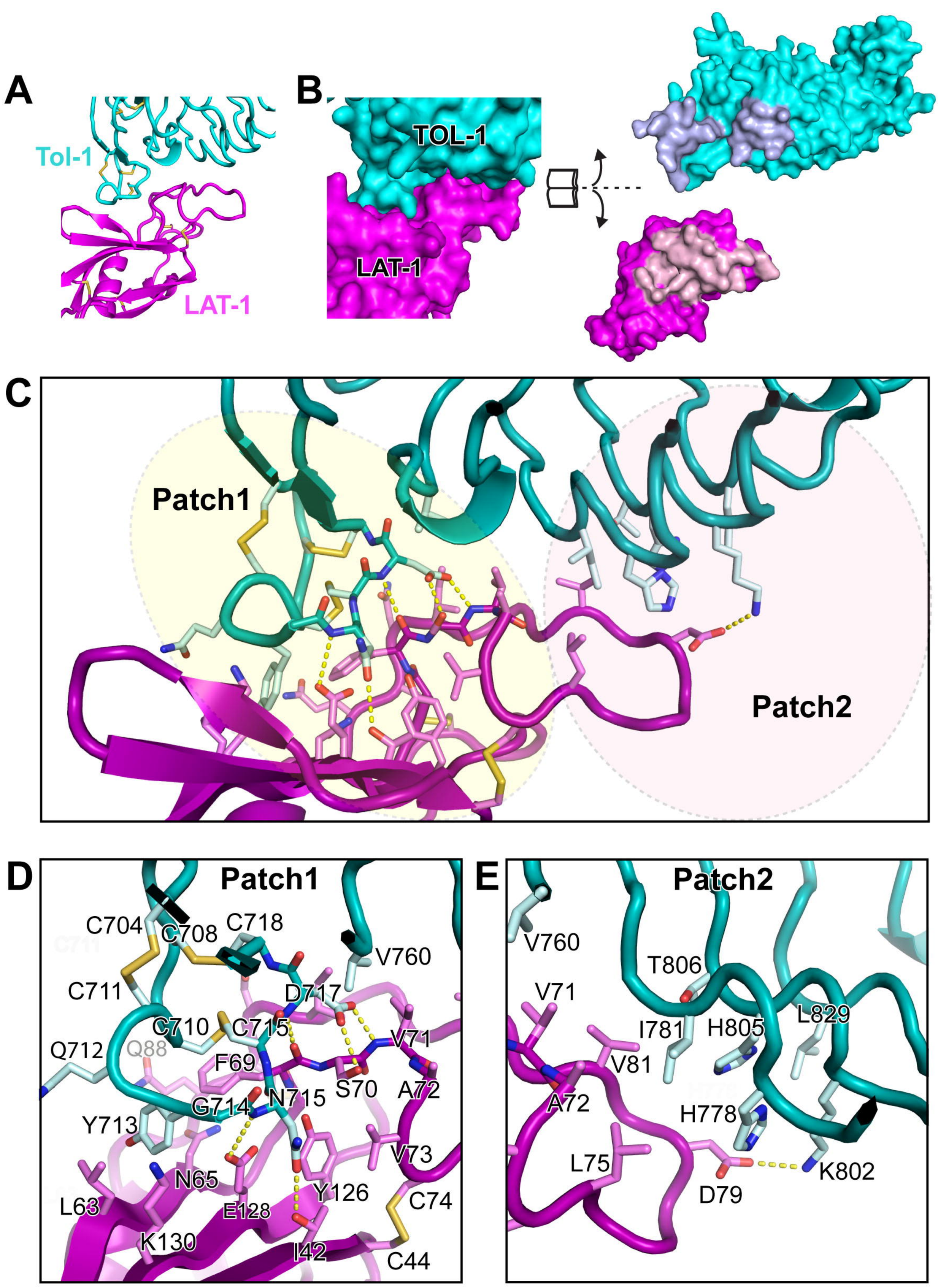

Carmona-Rosas et al., Figure 5

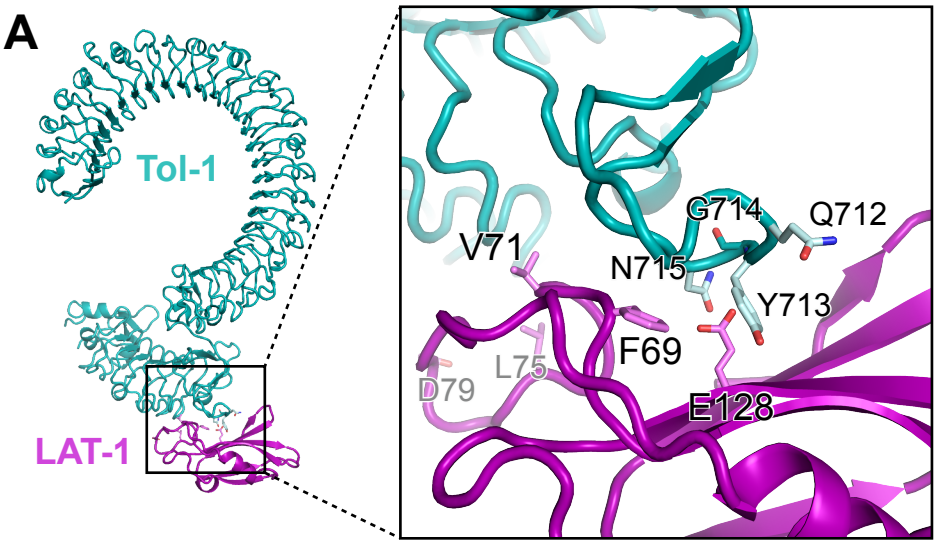

B

LAT-1 ECD _AP5 (Prey)

TOL-1 ECD _Fc (Bait)	WT	F69A	V71A	L75A	D79A	E128A
WT	0.433	0.040	0.331	0.502	0.213	0.275
Q712A, Y713A G714A, N715A	0.041	0.040	0.042	0.040	0.040	0.040
ΔN-LRR	0.297	0.040	0.251	0.344	0.195	0.178
ΔC-LRR	0.040	0.040	0.039	0.040	0.040	0.040

Abs (650 nm).

0.5
0.4
0.3
0.2
0.1

Carmona-Rosas et al., Figure 6

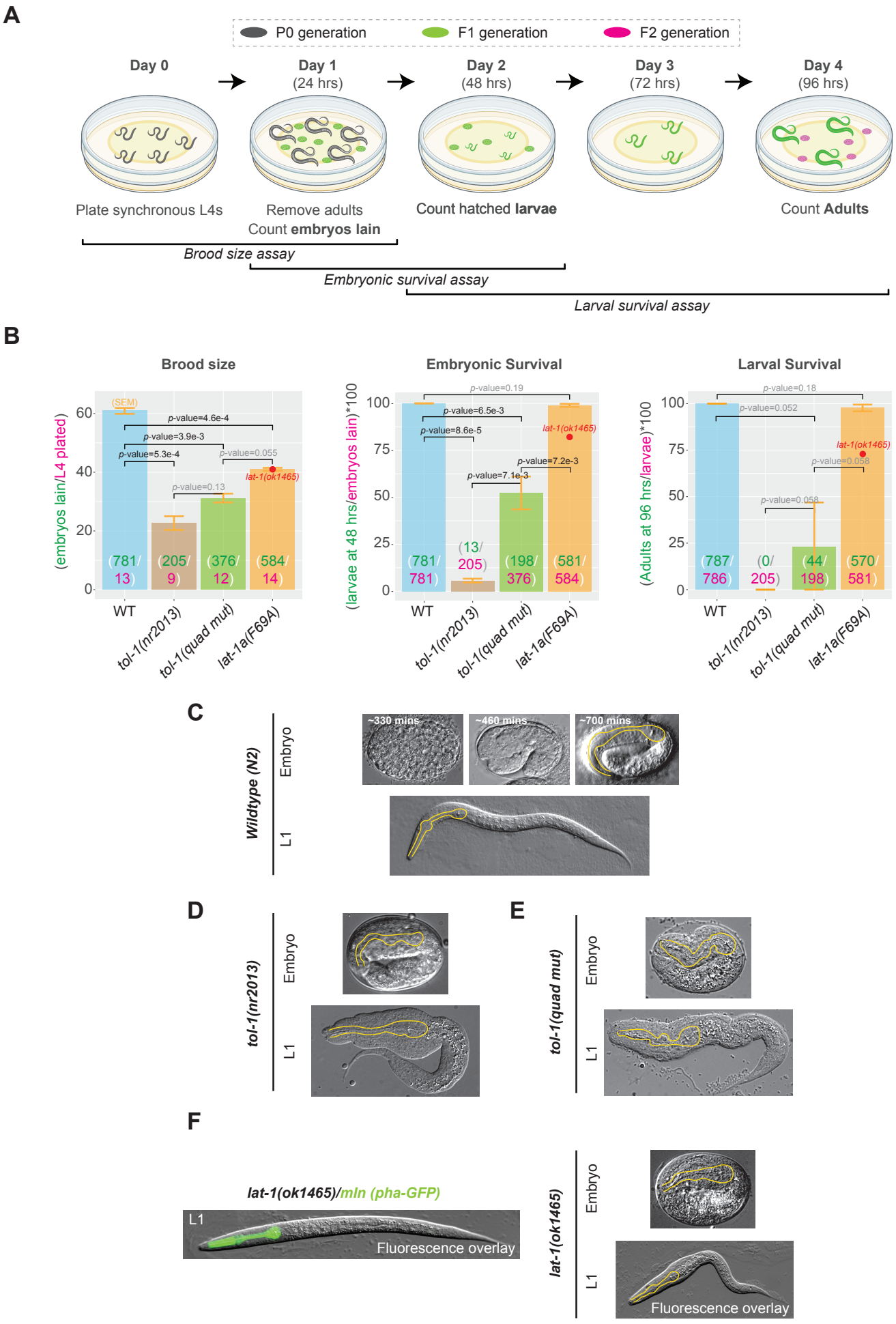
A
P0 generation
F1 generation
F2 generation
Day 0
Day 1 (24 hrs)
Day 2 (48 hrs)
Day 3 (72 hrs)
Day 4 (96 hrs)
Plate synchronous L4s
Remove adults
Count embryos lain
Count hatched larvae
Count Adults
Brood size assay
Embryonic survival assay
Larval survival assay
B
Brood size
Embryonic Survival
Larval Survival
(embryos lain/L4 plated)
(larvae at 48 hrs/embryos lain)*100
(Adults at 96 hrs/larvae)*100
(SEM)
p-value=4.6e-4
p-value=3.9e-3
p-value=5.3e-4
p-value=0.055
p-value=0.13
lat-1(ok1465)
(781/13)
(205/9)
(376/12)
(584/14)
p-value=0.19
p-value=6.5e-3
p-value=8.6e-5
p-value=7.2e-3
p-value=7.1e-3
(781/781)
(13/205)
(198/376)
(581/584)
p-value=0.18
p-value=0.052
p-value=0.058
p-value=0.058
(787/786)
(0/205)
(44/198)
(570/581)
WT
tol-1(nr2013)
tol-1(quad mut)
lat-1a(F69A)
C
Wildtype (N2)
Embryo
L1
~330 mins
~460 mins
~700 mins
D
tol-1(nr2013)
Embryo
L1
E
tol-1(quad mut)
Embryo
L1
F
lat-1(ok1465)/mln (pha-GFP)
L1
Fluorescence overlay
lat-1(ok1465)
Embryo
L1
Fluorescence overlay

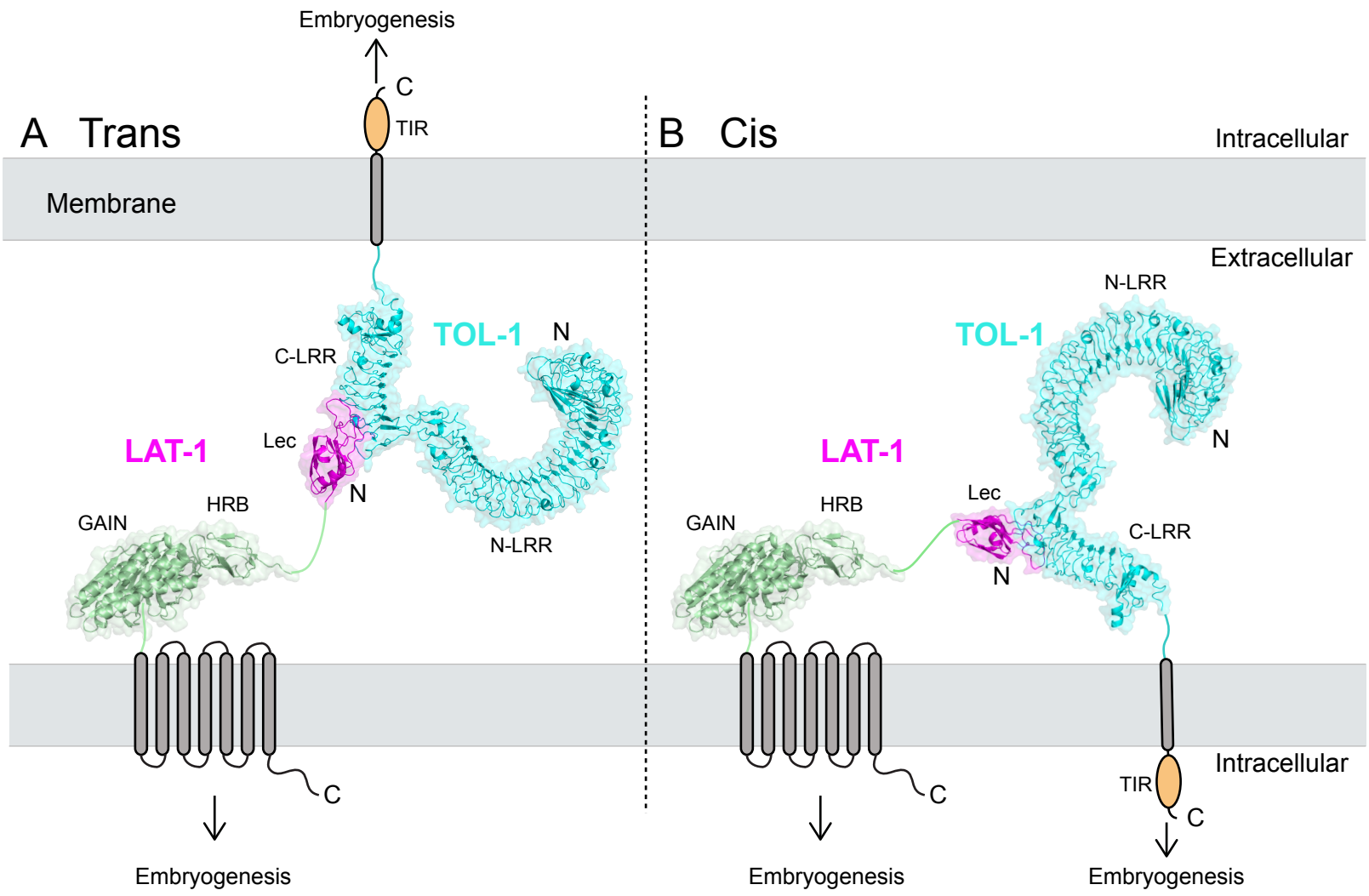

Carmona-Rosas et al., Figure 8